Gas and Liquid Distribution in the Monolith Film Flow Reactor

Achim K. Heibel
Corning Inc., Corning Environmental Technologies, Corning, NY 14831

Frank J. Vergeldt and Henk van As
Wageningen NMR Centre, Laboratory of Biophysics, 6703 HA Wagenigen, The Netherlands

Freek Kapteijn and Jacob Moulijn
Delft ChemTech, Industrial Catalysis, Delft University of Technology, 2628 BL Delft, The Netherlands

Thorsten Boger
Corning GmbH, 65189 Wiesbaden, Germany

The gas-liquid distribution in a monolith film flow reactor is investigated in the scope of this work. Magnetic resonance imaging (MRI) and a customized liquid collection method have been successfully applied to determine the liquid distribution over the monolith cross-section. Using a well-positioned spray nozzle liquid distributor, very uniform distributions are found which address the needs for applications that require high single-pass conversions. Due to the lack of radial convective flow in monoliths, the initial distribution propagates through the reactor. With a correct positioned spray nozzle distributor, a far more uniform distribution than the "natural" one for trickle beds is obtained. MRI, applied to study the local gas-liquid distribution in a monolith channel, clearly shows the accumulation of the liquid in the corners of the individual channel with an arc-shaped gas-liquid interface. Differences in local liquid holdup over the channel corners were found, which is described as channel scale nonuniformities. The experimental results are in good agreement with a fundamental hydrodynamic model based on the Navier-Stokes equations. The average liquid saturation is conveniently described with an engineering correlation $\beta_L = 6.6 \cdot (Fr_{Ls}^2/Re_{Ls})^{0.46}$*, as a function of the liquid phase Reynolds and Froude number.*

Introduction

Recently, the application of monolithic structures has been extended to multiphase gas-liquid-solid systems. Two different flow regimes are the main focus of research here. In Taylor or bubble-train-flow gas bubbles separated by liquid plugs pass through the individual channels of the monolith. Taylor flow monolith reactors can be operated in co-current upflow and downflow mode. A gas to liquid ratio between one to three is proposed to facilitate stable Taylor flow with superficial liquid velocities ranging from 0.05 to 0.15 m/s (Andersson et al., 1998). Usually monoliths with a channel diameter less than 2 mm are applied.

On the other hand, it is also feasible to operate the monolith reactor in the film flow regime. In this case the liquid flows down the channel walls, whereas the gas occupies the core of the channel. The separated flow passages of gas and liquid allow both co- and countercurrent operation of the film flow monolith reactor. The channel dimensions are usually smaller than 5 mm and superficial liquid velocities up to 0.05 m/s are applied with a gas to liquid ratio of up to 20.

Flow distribution is a general concern in multiphase operations. The impact of flow distribution effects always involves two aspects. On the one hand, the distribution is determined from a hydrodynamic perspective and on the other hand the impact on the reactive or separation performance is evaluated. A majority of the work concerning flow distribution concentrated on separation and absorption applications (such

Correspondence concerning this article should be addressed to A. K. Heibel at this current address: Corning, Inc., HB-CB-02, Corning, NY 14831.

as distillation columns) (Kister, 1989; Perry et al., 1990; Olsson, 1999). For these operations, the uniformity of the phase distribution was also linked to the performance and the impact on separation efficiency (Porter and Jones, 1987; Bonilla, 1993; Higler et al., 1999).

Other studies focused on flow distribution in reactor systems, especially for trickle beds (Marchot et al., 1999). The reactants in the liquid phase are usually converted with an excess of the stoichiometrically required gas components. Therefore, the uniform distribution of the liquid phase is generally of more interest. With a good liquid-phase distribution, the uniform distribution of the pressure-driven gas flow is rather likely. The interaction of gravity, inertia, viscous and capillary forces increase the complexity of the liquid-phase distribution phenomena.

Generally, different scales with their specific resolutions are considered in distribution evaluations. For trickle beds and packed bed columns, two different scales have been established (Hoek et al., 1986; Zuiderweg et al., 1987). On a column scale, the distribution over the cross section is considered. For round columns, the distribution at a given cross section is only a function of the radius. Heterogeneity in the bed (such as wall effects) and initial distribution issues are the dominating phenomena on column scale. On the other hand, a certain resolution of the measurement technique in space is necessary to sufficiently resolve the particle-scale maldistribution. These small-scale distribution differences result from the preferential flow of rivulets through the bed, which show a much stronger dependency on the gas- and liquid-flow rate, compared to the column scale (Wang et al., 1998).

Due to the radial dispersion in trickle beds and corrugated sheet packings, the flow distribution can change over the column height. Indeed, it is suggested that each packing structure has a "natural" distribution, which will be obtained after a certain packing height. The required packing height will depend on the deviation of the initial distribution from the natural distribution and the radial spreading coefficient (Wang et al., 1998), which is a function of the packing structure. Initial distributions more uniform than the "natural" distribution will deteriorate to the "natural" one with the reactor length. For the monolith reactor, liquid distribution is very important, due to the limited flow exchange perpendicular to the channel. A good initial distribution is necessary, which will be maintained throughout the reactor. Similar to the different scales of distribution for trickle beds, the flow distribution for monoliths can be also investigated in different detail. On a monolith scale, the distribution of the fluids over the entire cross-section or all of the channels is of interest, which can be compared to the particle scale of trickle beds. On a more microscopic level, the gas- and liquid-phase distribution inside the individual channel is a vital input for a good mathematical description of the hydrodynamic and mass-transfer phenomena. The microscopic level can be described as a channel scale.

Different experimental methods have been utilized to investigate the hydrodynamics in multiphase reactors. Basically, we can differentiate between conventional collecting and tomography methods. The collecting techniques are rather straightforward by local collection of the liquid over the cross section of the reactor. The more sophisticated tomography methods are based on conductance, capacitance, optical, and X-ray tomography (Chaouki et al., 1997). Recently nuclear magnetic resonance imaging (MRI) has been applied to determine the flow field, the phase distribution, and mass-transfer phenomena in packed beds (Seymour et al., 1997; Tallarek et al., 1998; Manz et al., 1999; Sederman et al., 2001; Mantle et al., 2002).

The aim of this work is to investigate the two-dimensional (2-D) liquid distribution over the cross-section of the monolith (monolith scale) by means of MRI and a collection technique. The impact of co- and countercurrent gas flow, as well as the appropriate distributor selection and positioning, are determined. With a simple reactor model, the influence of liquid distribution on reactor performance is discussed.

In the second part MRI is used to determine the liquid distribution inside the individual channel (channel scale). Besides the qualitative information about the shape of the gas-liquid interface and the location of the liquid, quantification of the mean liquid holdup and its variations are of interest. Furthermore, a previously developed model of the flow field is evaluated using the experimental data.

Monolith Scale Investigations

Experimental

A 25 cells per square in. (cpsi) monolith with square channels of a hydraulic diameter of 4.11 mm was used for the experiments. A custom made distribution section was connected on the top of the monolith using a ϕ45 mm Acrylate tube. The monolith material is cordierite ($2MgO \cdot 2Al_2O_3 \cdot 5SiO_2$) with a bulk porosity of around 30%. The outer skin was sealed with a polymeric resin to prevent leakage to the outside. The monolith matrix under investigation consisted of 44 channels.

Water has been primarily used as liquid and air as gas phase (Table 1). Three different spray nozzle liquid distributors (Spraying Systems, Unijet & Fulljet series, TG-SS 0.4, QG-SS-1, QG-SS-3) were applied to cover the liquid flow range of interest. A gear pump (Micropump, Series 223) circulated the liquid and the flow was measured via a turbine flow sensor (Digi-flow systems, DFS-2, $\pm 1\%$ full scale). For the experiments with forced gas flow, the air was supplied by a mass-flow controller (Brooks Instruments, 5853S, $\pm 1\%$ full scale). All measurements were performed at room temperature and ambient pressure. Before all experiments, the monoliths were wetted with a high liquid flow for a period of 30 min.

In Figure 1a the MRI experimental setup is illustrated. A monolith length of 500 mm was used for the MRI measurements; details of the experimental technique are discussed

Table 1. Fluid Properties at 20°C and 1.015 bar_a (Janssen et al., 1991; Hikita et al., 1978)

	Dyn. Viscosity [Pa·s]	Density [kg/m^3]
Water	1.00×10^{-3}	998
10% sucrose in water	1.36×10^{-3}	1,038
25% sucrose in water	2.29×10^{-3}	1,104
Air	0.018×10^{-3}	1.20

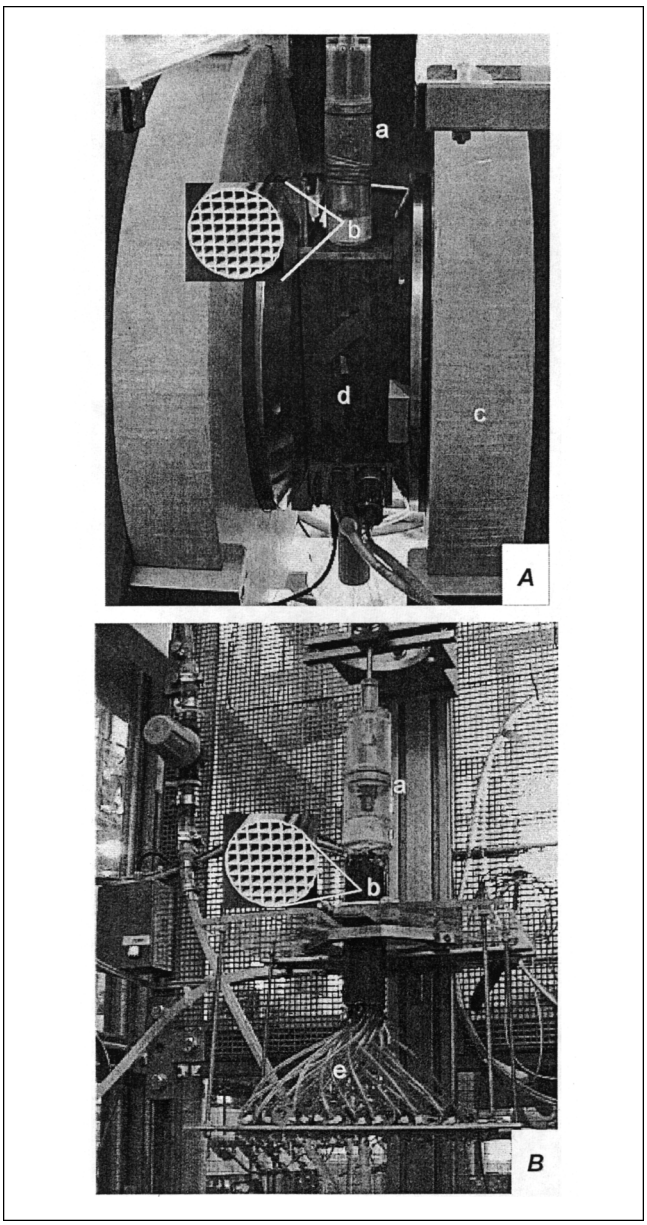

Figure 1. Experimental setups: (A) MRI and (B) collection.

(a) Liquid distribution section; (b) monolith test section; (c) main magnet coil; (d) gradient set with secondary coil; (e) liquid collection section.

elsewhere (Heibel et al., 2001b). Magnetic resonance imaging was performed with an image matrix of 128×128 pixels, which results in an inplane resolution of approximately 0.4 mm. Additional MRI parameters are given elsewhere (Heibel et al., 2001b).

For the liquid distribution measurements, Tygon tubes were inserted in each channel of a 250 mm long monolith (Figure 1b). The opposite ends of the tube were mounted on a plate. A tray with the same number of containers (25 mL) as monolith channels fitted accurately under the plate to collect the liquid from each individual tube. The liquid was collected in the containers over a certain period of time, and, afterwards, the volume in each container was determined. This allowed the calculation of the average liquid velocity in each channel during the time period of liquid collection. However, the measurement method did not allow the introduction of any gas flow, especially not countercurrently. To understand the impact of gas flow on liquid distribution, some preliminary MRI experiments with and without gas flow have been performed. The gas flow was set to a rather high value to expose the liquid film to a high shear rate. Both co- and countercurrent operations have been investigated. The results did not reveal any detectable differences in the liquid flow pattern due to the applied gas flow, which seems reasonable for the low interaction film flow regime. Therefore, the rest of the experiments have been performed without any forced gas flow.

Impact of distributor

The amplitude of the MRI signal representing the local water density over the entire monolith shows three distinct regions (Figure 2): the gas region in the center (no amplitude), the flowing liquid in the corners of the channels (high amplitude) and the trapped liquid in the porous walls (low amplitude). Two effects cause the low amplitude in the wall areas. On the one hand, the maximum liquid holdup in the wall is restricted by the material porosity (30%), so that the actual water or, better, the proton density, is much lower compared to the filled area in the channel. On the other hand, the water molecules in the wall have a very short relaxation time, due to the interaction with the surrounding solid structure (Heibel et al., 2001b). Under the applied film flow operation, the preferential flow of the liquid in the corners ("corner flow") of the channel is clearly visible. In general a good liquid distribution is observed especially for distributor QG-SS-1 and QG-SS-3, which is in agreement with the collection testing. For distributor TG-SS-04, both test methods resulted in a liquid deficiency in the center of the monolith, which gives additional confidence in the experimental techniques. Furthermore, the images imply that higher liquid velocities result in a higher liquid holdup. Additionally, differences in the size of the liquid pockets in a single channel can be determined, but a higher resolution is necessary to allow for quantitative conclusions. The distortions in the amplitude images are caused by the nonlinearity of the magnetic field gradient (especially on the bottom left side of the images). These distortions were experienced throughout all measurements with a large field of view (50 mm), but do not impact the qualitative analysis of the MRI data.

Impact of distributor positioning

Besides the appropriate selection of the distributor, it is also necessary to position the distributor correctly to the top face of the monolith. Therefore, a series of experiments with different positioning of the distributor have been performed (Figure 3). Again, good qualitative agreement between MRI testing and the collection test method is found. Wrong positioning of the distributor has significant effects on the uniformity of the distribution. A too high positioning results in

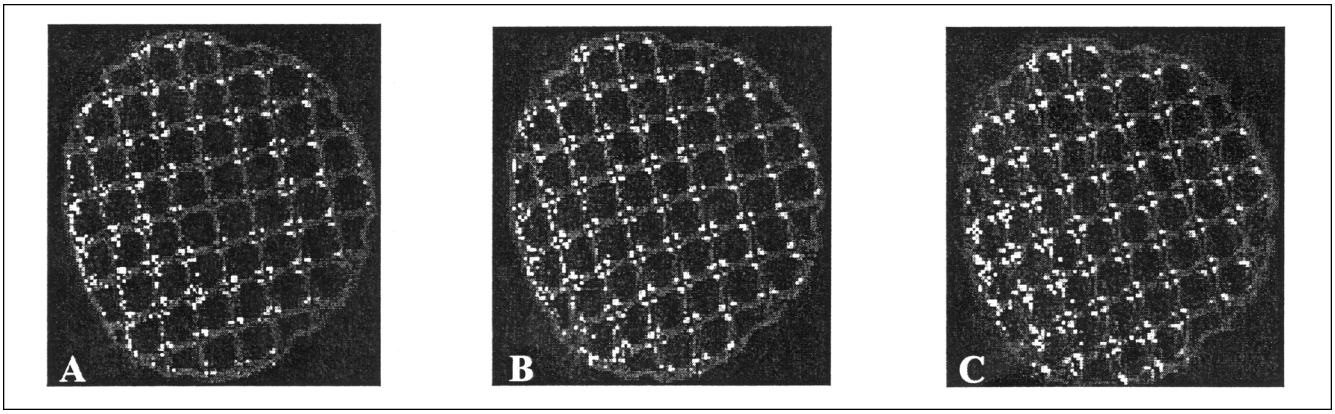

Figure 2. Monolith-scale MRI images, bright colors represent high liquid density, dark colors represent low liquid density, black color represents gas phase.

(A) $u_{Ls} = 0.75$ cm/s distributor TG-SS-0.4; (B) $u_{Ls} = 0.95$ cm/s distributor QG-SS-1; (C) $u_{Ls} = 2.25$ cm/s distributor QG-SS-3.

significant wall flow and a too low positioning in an area of high flow in the center of the monolith. Due to this sensitivity, prior to any hydrodynamic or reactive investigation, the optimum distributor position has been determined for three different flow rates to minimize the distribution effects on the performance.

Quantitative analysis

An important feature of the applied collection technique is the possibility of a quantitative analysis of the distribution performance. A commonly used index to describe distribution is the hydrodynamic maldistribution factor (Hoek et al., 1986)

$$M_h = \frac{1}{A} \cdot \iint \left(\frac{u_{\text{loc}} - u_{\text{avg}}}{u_{\text{avg}}} \right)^2 dA \qquad (1)$$

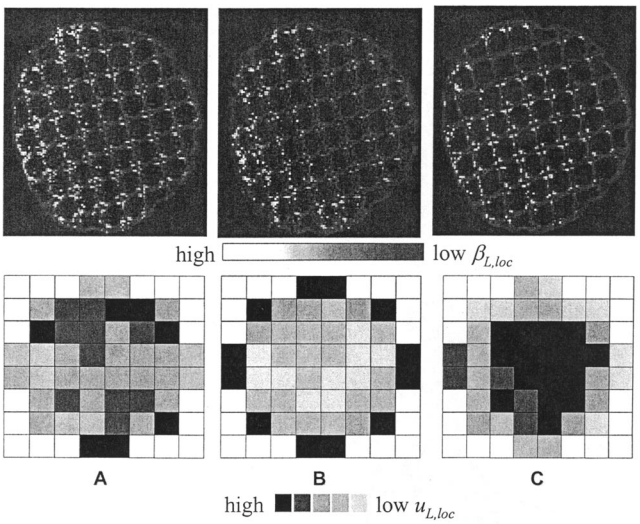

Figure 3. Monolith-scale MRI images and results of collection method for different positions of Distributor QG-SS-1 at $u_{Ls} = 1.7$ cm/s.

(A) Optimum position (30 mm), $M_h = 0.075$; (B) too high positioned (40 mm), $M_h = 0.215$; and (C) too low positioned (20 mm), $M_h = 0.275$.

For a uniform flow, the hydrodynamic maldistribution factor has a value of zero, and increasing values indicate a larger deviation from uniformity.

In Figure 4A a typical graph showing the dependency of nozzle position on the maldistribution factor is illustrated. Obviously, there is an optimum distributor height, which results in the best distribution. The critical distributor position is a function of the flow rate, the fluid system, and the distributor itself. Furthermore, slight variations between distributors of the same construction have been detected.

Applying the optimum distributor position, the distribution pattern is evaluated for different liquid flow rates (Figure 4b). The distribution uniformity improves for higher flow rates. Indeed, the improvement in uniformity is seen as a function of the flow rate rather than the superficial reactor velocity, due to the fact that the monolith mostly propagates the initial distribution through the reactor and the applied distributor system is rather sensitive to liquid flow rate. Therefore, an even better distribution at lower superficial reactor velocities can be achieved, if the cross-sectional area of the reactor is enlarged. Experiments with decane as liquid showed similar behavior (Heibel et al., 2001a) indicating that, for the selected distributor, the surface tension is not very critical, which is in agreement with the documentation of the manufacturer.

The distribution behavior of monoliths is rather different from the one of trickle beds, which develop their own "natural distribution" after a certain length, due to the radial flow exchange. Typical maldistribution factors for trickle beds range around 0.3 to 0.5 for larger particles (10–50 mm) (Hoek et al., 1986) and from 0.175 to 0.65 for smaller particles (3 mm) (Wang et al., 1998), also depending on the bed height.

With a good initial flow distribution, the monolith reactor can be operated with an extremely uniform flow distribution, which is maintained throughout the reactor.

Impact on reactor performance

The distribution patterns described above only consider the hydrodynamic aspects. Finally, the impact on reactor performance is of much more importance and interest. Therefore, a simple case of a chemical reaction of species A converted to

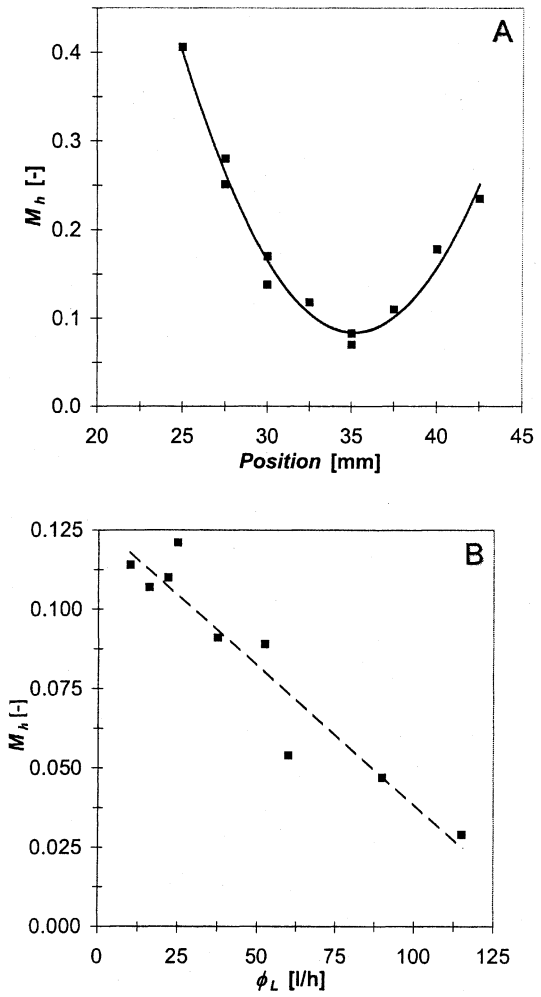

Figure 4. Hydrodynamic maldistribution factor M_h as a function of (A) distributor position ($\phi_L = 35$ L/h) and (B) liquid flow rate for optimum distributor position.

Lines represent best fit.

species B is considered. Only the liquid phase is considered, due to the fact that for most of the applications of interest the gas reactant is in excess (Lebens, 1999). Under the assumption of first-order reaction kinetics and plug-flow behavior in the channel, the remainder or the amount of unconverted reactant follows to

$$\frac{c_{l,ch}}{c_{\text{in}}} = e^{[-(k\cdot l)/u_{L0,ch}]} \tag{2}$$

The assumption of a constant activity k independent of the liquid flow rate is valid, if external mass transfer and wetting phenomena do not affect the reactor performance (Carruthers and DiCamillo, 1988). Furthermore, an isothermal system is assumed, independent of the flow distribution.

Due to the lack of exchange between the individual channels of the monolith, each channel operates as an individual reactor. The mixing cup concentration at the outlet is obtained by integration over the cross section

$$\frac{c_l}{c_{\text{in}}} = \frac{\iint \frac{c_{l,ch}}{c_{\text{in}}} \cdot u_{L0,ch} \cdot dA}{\iint u_{L0,ch} \cdot dA} \tag{3}$$

An obvious way to quantify the difference in performance between uniform and maldistributed flow is to compare the conversion for both cases

$$\Delta\xi = \frac{c_{l,\text{mal}} - c_{l,\text{uni}}}{c_{\text{in}}} \tag{4}$$

This measure is especially useful for reactor configurations operating at low to medium conversion levels, like recycle reactors. However, for reactors operating at high conversions, like single-pass configurations, the situation is somewhat different. Here, the performance differences are better assessed by considering the amount of unconverted species, also called the remainder, compared to the ideal case. Therefore, the reactive maldistribution factor is introduced

$$M_R = \frac{c_{l,\text{mal}} - c_{l,\text{uni}}}{c_{l,\text{uni}}} \tag{5}$$

which represents the difference in unconverted species of maldistributed and uniform flow relative to the remainder for uniform flow. Similar to the hydrodynamic maldistribution factor (Eq. 3), this factor has a value of zero for uniform utilization of the reactor cross section and increases with increasing nonuniformity.

Figure 5A illustrates the impact of maldistribution on reactive performance as a function of the dimensionless group $k\cdot l/u_{L0}$. A value of 7 for this parameter corresponds to a conversion of 99.9% in the case of uniform flow. As expected, the performance decreases significantly with larger deviations from uniform flow. The difference in conversion shows a maximum around a $k\cdot l/u_{L0}$ value of 2, independent of the value of the maldistribution factor. At lower $k\cdot l/u_{L0}$ values, the conversion is overall low and, therefore, only a small detrimental effect is apparent. On the other hand, for high values or high conversions, both cases of uniform and maldistributed flow converge towards a value of unity and again the difference in conversion is approaching zero. Between these two bounding regimes, a maximum difference in conversion is obtained. The maximum difference in conversion and the corresponding $k\cdot l/u_{L0}$ value of 2 can be, for example, utilized in a reactive test to determine distribution biased performance with adequate experimental resolution.

For high conversion reactors, this maximum difference is of rather limited importance. Here, the ratio between the unconverted species for uniform and maldistributed flow has much more impact (Eq. 5). Figure 5A clearly indicates that the uniform distribution of liquid becomes more critical as the $k\cdot l/u_{L0}$ value or the conversion increases.

For the distribution patterns illustrated in Figure 4B, a maximum value of a hydrodynamic maldistribution factor of

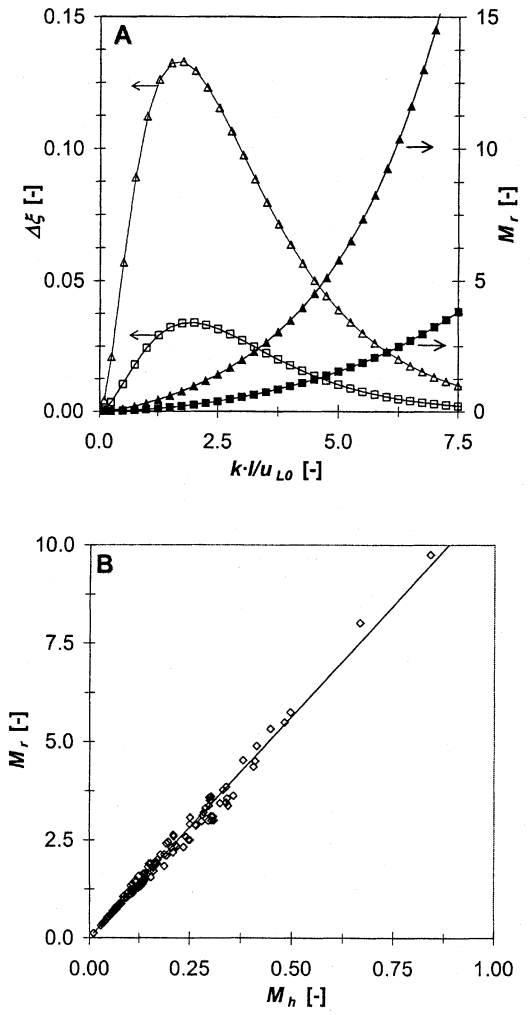

Figure 5. Impact of maldistribution on reactor performance.

(A) Maldistribution parameters $\Delta\xi$ and M_r as a function of $k \cdot l/u_{L0}$ for hydrodynamic maldistribution factors of 0.125 (□/■) and 0.5 (△/▲). (B) Reactive maldistribution parameter M_r as a function of the hydrodynamic maldistribution factor of measured distribution patterns for a conversion of 99% under uniform flow. Lines represent best fit.

0.125 represents the worst case. For a targeted conversion of 99.9% under uniform flow, this results in a roughly four-fold higher remainder than desired, which seems to be reasonable for these stringent requirements.

An infinite number of distribution patterns can result in the same hydrodynamic maldistribution factor. Therefore, it is important to evaluate the suitability of this lumped factor for the description of the reactive performance. A total number of 140 measured distribution patterns over a broad range of nonuniformity have been considered and the functional dependency between the hydrodynamic and reactive maldistribution factor was determined (Figure 5B). The two maldistribution factors correlate very well. The graph illustrates the results for a conversion of 99% under uniform flow. In general, for all conversion levels, a linear relationship between the two maldistribution factors is found. However, for conversion higher than 99.5%, the correlation shows significantly more spread for higher values of the hydrodynamic maldistribution factor ($M_h > 0.20$).

In summary, the hydrodynamic maldistribution factor seems to be a proper index to describe the flow distribution with respect to reactor performance. Especially at lower values of the hydrodynamic maldistribution factor, which is the interesting area for monoliths, the correlation is outstanding.

Channel Scale Investigations

The monolith scale MRI experiments revealed that the liquid accumulates in the corners of the square channels of the monolith. This resolution was not high enough to quantify the size of the liquid pockets and the shape of the gas-liquid interface. Both parameters are important inputs for an accurate description of the flow and transport phenomena in the monolith channel. An adapted experimental procedure allowed determining the liquid distribution in the channel and comparing it to a fundamental physical model.

Experimental

For the channel scale experiments, the outer channels were removed over 2/3 of the monolith length and only four channels (2×2) in the center were kept over the entire length of

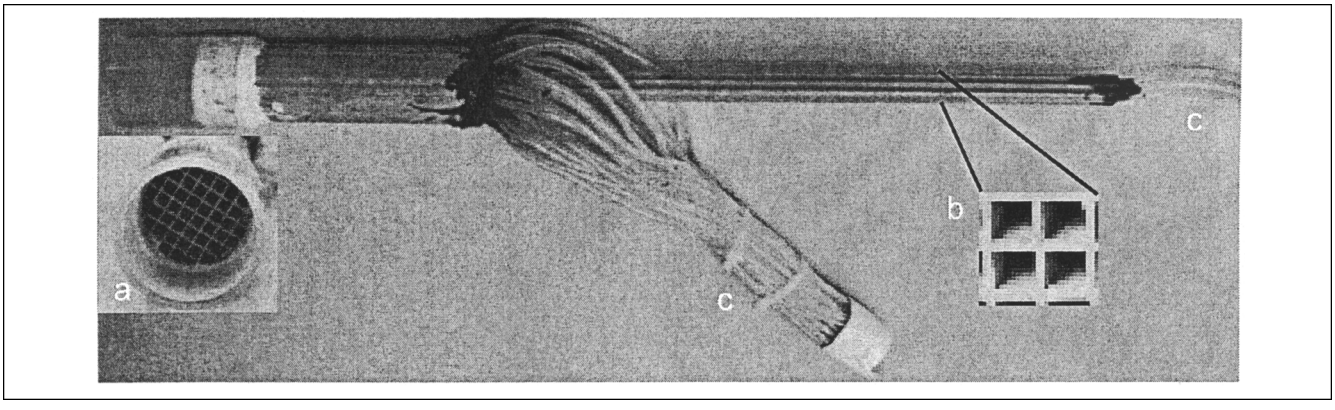

Figure 6. Channel scale test section.

(a) Liquid distribution section; (b) monolith test section; (c) liquid drainage tubes.

Cell Density [cpsi]	25	50
Diameter [m]	0.043	0.043
Void fraction [%]	67	68
S/V ratio [m²/m³]	654	939
d_h [mm]	4.12	2.91

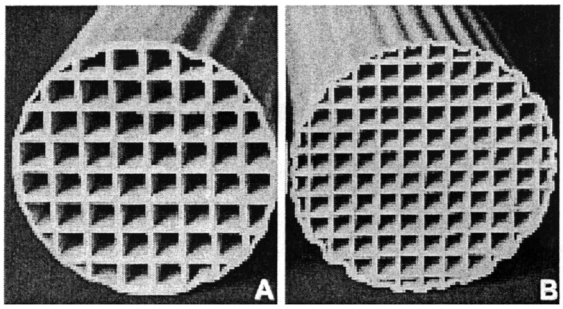

Figure 7. Geometry properties of the monoliths.
(A) 25 cpsi; (B) 50 cpsi monolith.

500 mm (Figure 6). Two different channel sizes have been investigated representing 25 cpsi monoliths ($d_h = 4.11$ mm) and 50 cpsi monoliths ($d_h = 2.91$ mm) (Figure 7). Inserting Tygon tubes in the individual channels drained the liquid flowing out of the outer region. This special preparation of the monolith allowed to use the standard liquid distribution devices described above and still be able to focus on individual channels and corners in the MRI measurement section. Furthermore, a sufficiently high resolution (≈ 70 μm) is obtained with MRI to determine the phase distributions in the individual channels. The experimental equipment to introduce the flow of gas and liquid through the monolith were identical to the ones described for the monolith scale experiments. Besides water, aqueous solutions with 10 and a 25 wt. % sucrose (Table 1) have also been used to determine the effect of liquid viscosity on the liquid holdup. Validation experiments with a single square glass channel and a glass rod in the center under stagnant liquid have been performed to proof the geometric accuracy of the MRI measurements of a similar liquid domain as experienced under the monolith film flow measurements (Heibel et al., 2001b). Furthermore, a binary gating image analysis method has been defined to distinguish between liquid and solid phase.

The experimental setup did not allow for the introduction of countercurrent gas flow. As already validated for the monolith scale measurements, no strong interaction between gas and liquid is expected in the film flow regime. Therefore, it has been decided to perform the majority of the experiments without forced gas flow and only allow free suction by the spray and the gravity-driven liquid film. In some experiments forced co-current gas flow has been applied, which is explicitly stated for these cases.

Results and discussion

The general phase distribution in capillary-sized channels under film flow conditions was the subject of an earlier investigation (Heibel et al., 2001b). This work clearly showed the liquid accumulation in the channel corners. Furthermore, the gas-liquid interface exhibited an arc-shaped curvature and complete wetting seemed to occur at the gas-liquid-solid contact line. These qualitative conclusions were in very good agreement with experimental and theoretical results of previous research (Kolb, 1993; Lebens et al., 1999).

As an extension of the previous research, Figure 8 shows the magnetic resonance images for different liquid viscosities. Higher viscosities result in thicker films and therefore increased holdup, which is also in-line with previously reported results (Lebens et al., 1999).

Additionally, the results indicate that the liquid holdup in the individual channel corners can still be substantially different, despite the liquid distribution homogeneity over the monolith cross-section.

For quantification, the liquid saturation is considered, which is a function of the flow regime and the gas- and liquid-flow rates. The definition is given as the ratio between

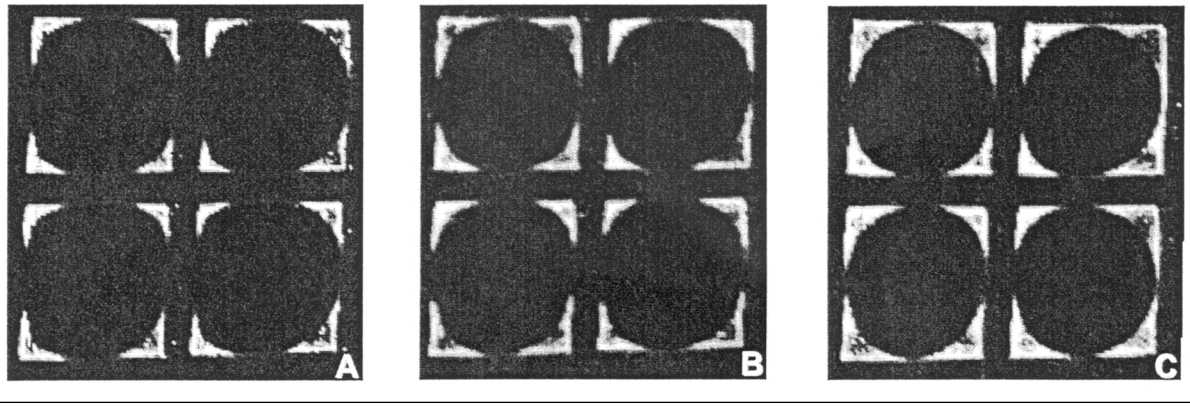

Figure 8. Magnetic resonance images for 25 cpsi monolith at $u_{Ls} = 3.2$ cm/s.
(A) Water ($\eta_L = 1.0 \times 10^{-3}$ Pa·s); (B) 10% sucrose in water ($\eta_L = 1.35 \times 10^{-3}$ Pa·s); (C) 25% sucrose in water ($\eta_L = 2.3 \times 10^{-3}$ Pa·s).

the liquid and the void area

$$\beta_L = \frac{A_L}{A_L + A_G} = \frac{A_L}{A_V} \tag{6}$$

The superficial liquid velocity is defined based on the void area of the channel

$$u_{Ls} = \frac{\phi_L}{A_V \cdot n_{ch}} \tag{7}$$

The MRI results allow for a localized analysis of the liquid saturation in the different corners of the monolith channels. Therefore, the amount of pixels in the corner of interest relative to the amount of pixels necessary to cover a quarter of the void of a channel is determined as the local liquid saturation (Figure 9A).

The average liquid saturation values over the four channels are presented as dotted lines for the three superficial liquid velocities considered. The liquid saturation in one channel is evenly spread around the average, confirming a rather uniform distribution between the four channels. However, the individual corners in a channel show a wide variation in local liquid saturation values. These variations show a systematic behavior, independent of the liquid superficial velocity. A valid hypothesis might be that at the monolith entrance, where the corner flow starts to develop the geometry differs slightly and, therefore, more or less liquid is guided into a corner. The initial distribution propagates downstream, without the ability to redistribute, due to the stable nature of the liquid pockets in the corner.

The average liquid saturation for the different fluids and conditions is compared in Figure 9B. Also shown are the predictions obtained by applying a physical model based on the Navier-Stokes equation for 1-D laminar flow of Newtonian fluids

$$\nabla \cdot (\eta \nabla u_{F,z}) = -\frac{dp}{dz} + g \cdot \rho \tag{8}$$

The assumptions and the details on the model are described elsewhere (Heibel et al., 2001b).

In general a good reproducibility of the measurements is given over the entire liquid flow range investigated, allowing the conclusion that the film is rather stable. An increase of the liquid saturation with superficial liquid velocity is apparent. However, this increase is nonlinear and flattens out for higher liquid velocities. For the fluids with higher viscosity, a higher liquid saturation is observed. The larger shear stress (proportional to the viscosity) reduces the maximum velocity in the liquid phase and results in a higher liquid holdup. Good qualitative, as well as quantitative, agreement with the model estimates are found. Deviations towards lower measured saturations are present for low superficial liquid velocities ($u_{Ls} < 0.75$ cm/s). Again, this is specific to the distributor, due to the maldistribution in the center region of the monolith as mentioned above (Figure 2A). The nonlinear dependency on the liquid velocity for higher velocities was previously investigated (Heibel et al., 2001b) and results from an overall higher

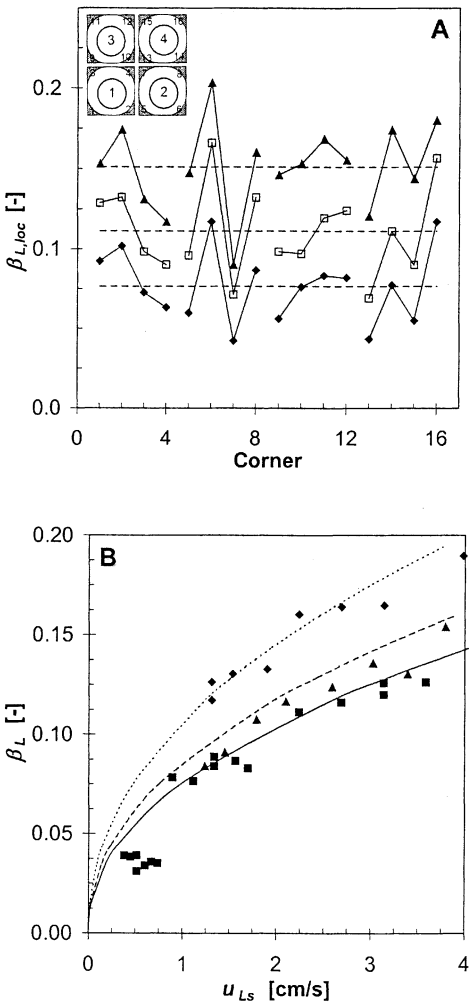

Figure 9. (A) Local liquid saturation $\beta_{L,loc}$ in the individual corners for different superficial liquid velocities u_{Ls}.

◆ 1.1 cm/s, □ 2.2 cm/s, ■ 4.0 cm/s, dashed line represents average liquid saturation; (B) liquid saturation β_L as a function of superficial liquid velocity for ■/— water ($\eta_L = 1.0$ Pa·s), ▲/--- 10% sucrose in water ($\eta_L = 1.35$ Pa·s) and ◆/··· 25% sucrose in water ($\eta_L = 2.3$ Pa·s). Lines represent model and symbols experimental data.

average film velocity, leading in a relatively lower liquid saturation.

In addition to the 25 cpsi monolith, experiments with a 50 cpsi monolith were also performed (Figures 10A,B). Compared to the results for the 25 cpsi monolith, higher liquid saturations were measured. This is a result of the larger *S/V*-ratio, which reduces the actual liquid velocities in the film. The comparison with the hydrodynamic model (Figure 10C) reveals good agreement between experiments and simulation.

Additionally, some experiments with a very high cocurrent gas flow have been performed (Figure 10C). In general, somewhat lower liquid saturation values were measured. This is in good agreement with the modeling data and results from the additional shear stress at the gas-liquid interface, which leads to a thinner liquid film and higher liquid velocities in the film. However, it should be mentioned that, despite the

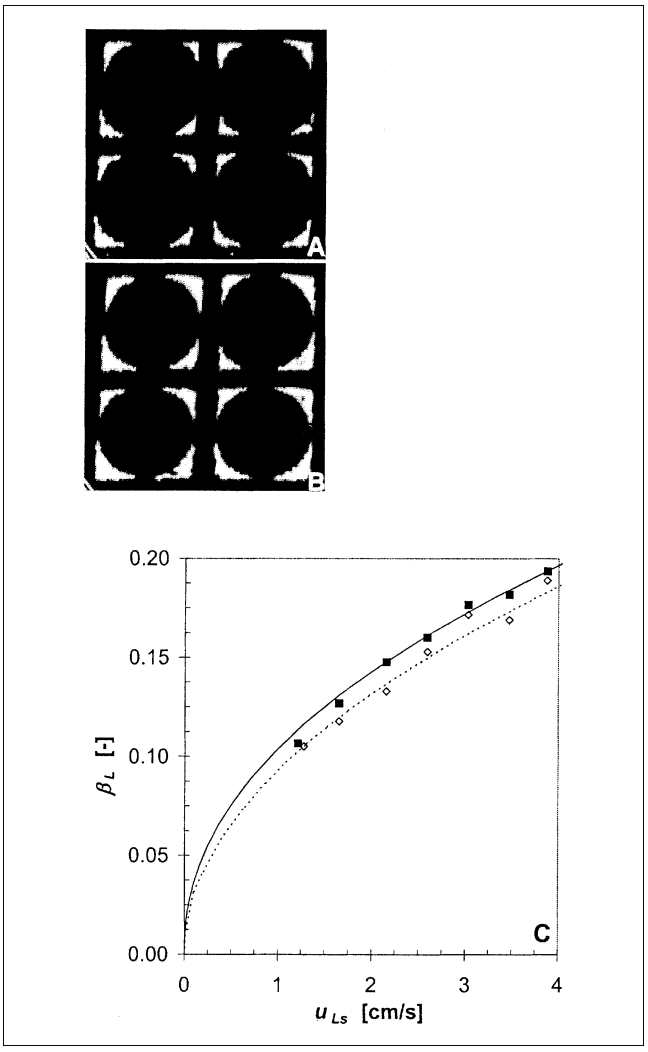

Figure 10. Magnetic resonance images for 50 cpsi monolith for (A) $u_{Ls} = 1.65$ cm/s and (B) $u_{Ls} = 3.85$ cm/s; (C) Liquid saturation as a function of superficial liquid velocity ■/— without forced gas flow and ◇/··· with forced cocurrent gas flow ($u_{Gs} = 2.7$ m/s).

All data for water/air. Lines represent model and symbols experimental data.

large co-current gas flows, the effect on the liquid saturation is rather limited. For an engineering correlation of the liquid saturation, it is sufficient to include only the effects of the liquid phase and neglect gas-phase effects.

A nondimensional form is chosen to summarize the dependency of the liquid saturation on liquid velocities and fluid properties. Lebens et al. (1999) found that the liquid saturation is conveniently described as a function of the ratio of Froude and Reynolds number, balancing the gravity, inertia, and viscous forces in the film. In Figure 11 all the experimental data for the liquid saturation are plotted as a function of the ratio of the dimensionless numbers (Fr_{Ls}^2/Re_{Ls}). The experimental data can be well described with Eq. 9

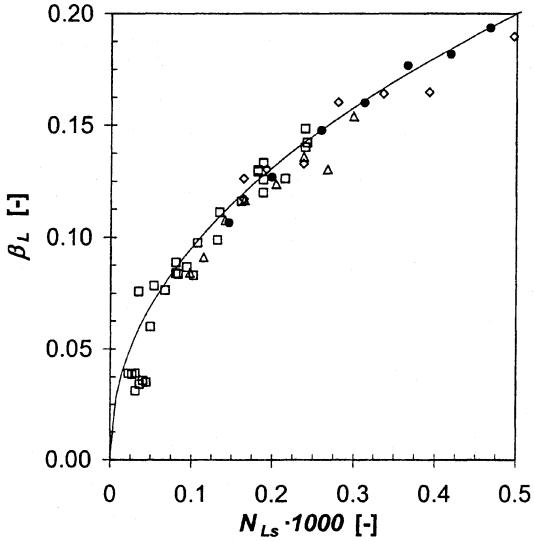

Figure 11. Liquid saturation as a function of $N_{Ls} = Fr_{Ls}^2/Re_{Ls}$ for 25 cpsi monolith for □ water, △ 10% sucrose in water, ◇ 25% sucrose in water, and ● 50 cpsi monolith for water, line represents correlation described by Eq. 9 with $C_1 = 6.6$ and $C_2 = 0.46$.

All experiments with free gas suction.

$$\beta_L = f\left(\frac{Fr_{Ls}^2}{Re_{Ls}}\right) = C_1 \cdot \left(\frac{Fr_{Ls}^2}{Re_{Ls}}\right)^{C_2} \tag{9}$$

A best fit for numerous model calculations result in values of 6.6 for C_1 and 0.46 for C_2, which are in good agreement with previously reported values (Lebens et al., 1999). The form of the dimensionless description is sufficient to describe the hydrodynamic effects on the liquid saturation.

Conclusions

Two different levels of distribution have been identified in the context of this work. On a monolith scale, the distribution over the different channels is of importance. MRI, as well as the collection method, showed good qualitative agreement and seems to be well suited to determine the distribution. The selection of the appropriate distributor and the positioning is of significant importance. The application of co- and countercurrent gas flow did not show any impact on the uniformity of the liquid phase over the monolith cross-section. The liquid distribution propagates over the length of the monolith, due to the lack of radial convective flow contributions. This behavior is different from trickle beds, which tend towards their "natural" distribution with reactor length. Therefore, more uniform distributions and, therefore, catalyst irrigation can be achieved and maintained in monoliths compared to trickle beds. The distribution effects can be conveniently described by a hydraulic maldistribution factor. The

impact of maldistribution on reactive performance was assessed for a first-order irreversible reaction. A reactive maldistribution factor, based on the unconverted species at the reactor outlet correlated very well with the hydraulic maldistribution factor, so both can be used as indicator for reactor performance. Maldistribution effects become more important for higher conversion levels. The very good distributions measured in the scope of this work can address the stringent requirements for high single-pass conversions.

On the channel level, it was found that the liquid accumulates in the corners of the channel. The gas-liquid interface is arc-shaped and complete wetting occurred at the G-L-S contact line. Despite the uniformity of the liquid distribution over the monolith cross-section, significant local nonuniformities over the different liquid pockets in the channel corners were found, which might result from local geometry differences at the monolith inlet section. The application of a high cocurrent gas flow leads to somewhat lower liquid holdups. The difference was not very significant, as expected for the low interaction flow regime.

The average liquid saturation increases nonlinearly with liquid velocity; furthermore, higher viscosity, as well as higher S/V ratio of the monolith packing, lead to higher holdups. The experimental data are in good agreement with a fundamental hydrodynamic model based on the Navier-Stokes equations for all the different parameters studied in the context of this work.

Due to the rather limited impact of the gas flow on the liquid saturation, a nondimensional description as a function of the liquid properties and channel dimensions is sufficient as an engineering correlation.

A good description of the experimental data is given by

$$\beta_L = 6.6 \cdot \left(\frac{Fr_{Ls}^2}{Re_{Ls}} \right)^{0.46} \tag{10}$$

relating the liquid saturation as a function of the Froude and Reynolds number.

Acknowledgments

The MRI work was performed at the Wageningen NMR Center at the Wageningen Agricultural University in The Netherlands. The support and technical input from Tom Scheenen and Ullrich Tallarek are highly appreciated. The work was in part supported by the EC TMR grant ERBFMGE-CT-950066 (access to EU large scale facility Wageningen NMR Center) and grant number HPRI-CT-1999-00085 (EC programme Access to Research Infrastructure).

Notation

A = area, m^2
c = concentration, mol/m^3
C_1, C_2 = constants (Eq. 9)
d = diamenter, m
g = gravitational constant, m/s^2
k = first-order reaction rate constant, $1/s$
l = length, m
M = maldistribution factor
n = number
p = pressure, Pa
r = radius, m
u = velocity, m/s
z = axial channel coordinate, m

Dimensionless groups

Fr = Froude number $\left(Fr = \frac{u}{\sqrt{g \cdot d_h}} \right)$
Re = Reynolds number $\left(Re = \frac{\rho \cdot u \cdot d_h}{\eta} \right)$

Greek letters

$\Delta\xi$ = difference in conversion
α = wetting angle, degree
β = liquid saturation, m_L^3/m_V^3
ϕ = volume flow rate, m^3/s
η = dynamic viscosity, $Pa \cdot s$
θ = half corner angle, degree
ρ = density, kg/m^3

Subscripts

uni = uniform
0 = reactor based
avg = average
c = capillary
ch = channel
F = fluid
G = gas
h = hydraulic
L = liquid
l = length
loc = local
mal = maldistributed
r = reactive
s = superficial
V = void
wet = wetted

Literature Cited

Andersson, B., S. Irandoust, and A. Cybulski, "Modeling of Monolith Reactors in Three-Phase Processes," *Structured Catalysts and Reactors*, Marcel Dekker, New York (1998).

Bonilla, J. A., "Don't Neglect Liquid Distribution," *Chem. Eng. Prog.*, **89**, 47 (1993).

Carruthers, J. D., and D. J. DiCamillo, "Pilot Plant Testing of Hydrotreating Catalysts," *Appl. Catal.*, **43**, 253 (1988).

Chaouki, J., F. Larachi, and M. P. Dudukovic, "Noninvasive Tomographic and Velocimetric Monitoring of Multiphase Flows," *Ind. Eng. Chem. Res.*, **36**, 4476 (1997).

Heibel, A. K., J. J. Heiszwolf, F. Kapteijn, and J. A. Moulijn, "Influence of Channel Geometry on Hydrodynamics and Mass Transfer in the Monolith Film Flow Reactor," *Catalysis Today*, **69**, 153 (2001a).

Heibel, A. K., T. W. J. Scheenen, J. J. Heiszwolf, H. VanAs, F. Kapteijn, and J. A. Moulijn, "Gas and Liquid Phase Distribution and Their Effect on Reactor Performance in the Monolith Film Flow Reactor," *Chem. Eng. Sci.*, **56**, 5935 (2001b).

Higler, A., R. Krishna, and R. Taylor, "Nonequilibrium Cell Model for Packed Distillation Columns—The Influence of Maldistribution," *Ind. Eng. Chem. Res.*, **38**, 3988 (1999).

Hikita, H., S. Asai, and Y. Azuma, "Solubility and Diffusivity of Oxygen in Aqueous Sucrose Solutions," *Can. J. Chem. Eng.*, **56**, 371 (1978).

Hoek, P. J., J. A. Wesselingh, and F. J. Zuiderweg, "Small Scale and Large Scale Liquid Maldistribution in Packed Columns," *Chem. Eng. Res. Des.*, **64**, 431 (1986).

Janssen, L. P. B. M., and M. M. C. G. Warmoeskerken, *Transport Phenomena Data Companion*, Delft University Press, Delft, The Netherlands (1991).

Kister, H. Z., *Distillation Operation*, McGraw-Hill, New York (1989).
Kolb, W. B., "The Coating of Monolithic Structures: Analysis of Flow Phenomena," PhD Thesis, The University of Tulsa (1993).
Lebens, P. J. M., "Development and Design of a Monolith Reactor for Gas-Liquid Countercurrent Operation," PhD Thesis, Technical University of Delft (1999).
Lebens, P. J. M., M. M. Stork, F. Kapteijn, S. T. Sie, and J. A. Moulijn, "Hydrodynamics and Mass Transfer Issues in a Countercurrent Gas-Liquid Internally Finned Monolith Reactor," *Chem. Eng. Sci.*, **54**, 2381 (1999).
Mantle, M. D., A. J. Sederman, L. F. Gladden, S. Raymahasay, J. M. Winterbottom, and E. H. Stitt, "Dynamic MRI Visualization of Two-Phase Flow in a Ceramic Monolith," *AIChE J.*, **48**, 909 (2002).
Manz, B., L. F. Gladden, and P. B. Warren, "Flow and Dispersion in Porous Media: Lattice-Boltzmann and NMR Studies," *AIChE J.*, **45**, 1845 (1999).
Marchot, P., D. Toye, M. Crine, A.-M. Pelsser, and G. L'Homme, "Investigation of Liquid Maldistribution in Packed Columns by X-Ray Tomography," *Trans. IChem. E*, **77**, 511 (1999).
Olsson, F. R., "Detect Distributor Effects Before They Cripple Columns," *Chem. Eng. Prog.*, **95**, 57 (1999).
Perry, D., D. E. Nutter, and A. H. Nutter, "Liquid Distribution for Optimum Packing Performance," *Chem. Eng. Prog.*, **86**, 30 (1990).
Porter, K. E., and M. C. Jones, "Liquid and Gas Distribution in the Scale-Up of Packed Columns," *IChemE Symp. Ser.*, **104**, A245 (1987).
Sederman, A. J., and L. F. Gladden, "Magnetic Resonance Imaging as a Quantitative Probe of Gas-Liquid Distribution and Wetting Efficiency in Trickle-Bed Reactors," *Chem. Eng. Sci.*, **56**, 2615 (2001).
Seymour, J. D., and P. T. Callaghan, "A Generalized Approach to the Measurement of Flow and Dispersion in a Porous Medium Using Nuclear Magnetic Resonance," *AIChE J.*, **43**, 2096 (1997).
Tallarek, U., D. van Dusschoten, H. VanAs, G. Guiochon, and E. Bayer, "Direct Observation of Fluid Mass Transfer Resistance in Porous Media by NMR Spectroscopy," *Angew. Chem., Int. Ed.*, **37**, 1882 (1998).
Wang, Y.-F., Z.-S. Mao, and J. Chen, "Scale and Variance of Radial Liquid Maldistribution in Trickle Beds," *Chem. Eng. Sci.*, **53**, 1153 (1998).
Zuiderweg, F. J., P. J. Hoek, and L. Lahm, "The Effect of Liquid Distribution and Redistribution on this Separating Efficiency of Packed Columns," *IChemE Symp. Ser.*, **104**, A217 (1987).

Manuscript received Apr. 10, 2002, revision received May 24, 2003, and final revision received Aug. 11, 2003.